Journal of Microscopy, Vol. 233, Pt 1 2009, pp. 18–23
Received 12 March 2008; accepted 22 July 2008

Method to deterministically study photonic nanostructures in different experimental instruments

B.H. HUSKEN*,†, L.A. WOLDERING†, C. BLUM‡ & W.L. VOS*,†
*Center for Nanophotonics, FOM Institute for Atomic and Molecular Physics (AMOLF), P.O. Box 41883, 1009 DB Amsterdam, The Netherlands
†Complex Photonic Systems (COPS), MESA+ Institute for Nanotechnology and Department of Science and Technology, University of Twente, P.O. Box 217, 7500 AE Enschede, The Netherlands
‡Biophysical Engineering Group (BPE), MESA+ Institute for Nanotechnology and Department of Science and Technology, University of Twente, P.O. Box 217, 7500 AE Enschede, The Netherlands

Key words. Alignment, cross-correlation, focused ion beam, meta-material, nanostructure, optical microscopy, scanning electron microscope.

Summary

We describe an experimental method to recover a single, deterministically fabricated nanostructure in various experimental instruments without the use of artificially fabricated markers, with the aim to study photonic structures. Therefore, a detailed map of the spatial surroundings of the nanostructure is made during the fabrication of the structure. These maps are made using a series of micrographs with successively decreasing magnifications. The graphs reveal intrinsic and characteristic geometric features that can subsequently be used in different setups to act as markers. As an illustration, we probe surface cavities with radii of 65 nm on a silica opal photonic crystal with various setups: a focused ion beam workstation; a scanning electron microscope (SEM); a wide field optical microscope and a confocal microscope. We use cross-correlation techniques to recover a small area imaged with the SEM in a large area photographed with the optical microscope, which provides a possible avenue to automatic searching. We show how both structural and optical reflectivity data can be obtained from one and the same nanostructure. Since our approach does not use artificial grids or markers, it is of particular interest for samples whose structure is not known *a priori*, like samples created solely by self-assembly. In addition, our method is not restricted to conducting samples.

Introduction

Nanotechnological developments are at the base of new applications in electronics, quantum information processing and nanophotonics. Many different nanometre sized structures have been fabricated and isolated for elaborate study (Tans *et al.*, 1997; Hla, 2005; Koppens *et al.*, 2006; López, 2006; Novotny & Hecht, 2006). An important class of nanostructures are so-called metamaterials (Smith *et al.*, 2004). These composite materials exhibit properties that depend, in particular, on their geometrical structure. The physical properties of nanostructures like metamaterials, single molecules and carbon nanotubes not only depend on their detailed structure but often also on their immediate vicinity. For experimental observations, it is therefore very important to be able to prepare a pre-defined structure and subsequently probe exactly that same structure.

In this paper, we are specifically interested in structures for optics. We consider a photonic sample in which nanometre sized regions of interest are fabricated. These nanostructures need to be examined in separate experimental setups. The various setups yield complementary information on the individually targeted nanostructures, for example, structural and optical reflectivity data. The ability to perform these experiments requires a deterministic approach to position and orient the structure with respect to the different experimental setups. Coordinates that can be obtained from translation stages in the setup are not sufficient to determine the exact position of the nanostructures under study. Therefore, additional control is needed.

In the semiconductor integrated circuit industry, position control of known structures is obtained by the creation of special markers on the wafers. These markers provide a firm alignment grid that is needed in the different fabrication steps of, for example, multilayered structures (Benkart *et al.*, 2005). The grid is also used to recover a certain position or nanostructure on a sample, see for example reference (Badolato *et al.*, 2005). Unfortunately, the process of artificial

Correspondence to: B.H. Husken. Tel: +31 206081234; fax: +31 206684106; e-mail: husken@amolf.nl

Table 1. Overview of the apparatus used with their corresponding magnifications, lateral resolutions and acceleration voltages.

	Magnification range		Lateral resolution (nm)	Used acceleration voltage (kV)
Apparatus	Min	Max		
FIB	37×	1 280 000×	7	30
SEM	40×	1 000 000×	3	1–1.5
Optical microscope	5×	100×	10^2	-
Home-built microscope	40×	40×	10^2	-

grid fabrication involves extensive and expensive production facilities that are not generally accessible. Furthermore, these grids may damage the structure, and grid fabrication is impossible if a sample needs to be created by self-assembly only, since their surroundings are not *a priori* known. In this paper, we show a different approach to recover the same region of interest. Our approach can even be applied to low-conductance samples. Intrinsic geometrical features in the vicinity of our nanostructure are used to act as position unique markers. These markers can be recovered in the images obtained from different experimental setups by use of, for example, cross-correlation techniques.

Experimental methods

Our structures under study consist of nanometre-sized hole arrays. These arrays are first milled on the surfaces of both polystyrene and silica opal photonic crystals (Woldering *et al.*, 2006). The opals with sphere radii of 111 (polystyrene) and 113 nm (silica) are grown by self-assembly on a glass microslide substrate, by use of the vertical controlled drying method (Jiang *et al.*, 1999). Prior to milling, carbon was deposited on the surface of the opal with a Bio-Rad E6700 Turbo Coater operating at a current of 50 A. Carbon layers have typical thicknesses of about 10 nm and assist in removing charges from the milled area.

To fabricate the nanostructures, the carbon coated opal is subsequently placed inside a focused ion beam workstation (FIB, xT Nova Nanolab 600, FEI, Eindhoven, The Netherlands). Use is made of a gallium ion beam accelerated at 30 kV and a beam current of 9.7 pA. The focus of the ion beam had a diameter of about 20 nm. The defects were milled with the ion beam by writing circular patterns with a diameter of 120 nm, positioned on the centre of the sphere. Arrays were milled intermittently. This means that between each milling step of 5 s, milling was stopped for approximately 10 s to promote redistribution of charges away from the processed area. Together with the applied carbon layers, this approach prevents charge build-up of the milled area, which typically results in beam drift and substantial damage to the opal. All single defects that are part of the array, are milled in parallel.

It is advantageous to align the sample's substrate edges parallel to the (x,y) translation axes of the sample positioner, as many experimental setups use translation stages. Spatial (x,y) coordinates relative to two corners of the substrate are used to identify the location where the material nanocavities are created, with a precision of about 50 μm. The sample is monitored during the FIB process at a high magnification of typically 65 000 times, using an Everhart Thornley secondary electron detector (ETD). This *in situ* imaging uses the same acceleration voltage and beam current as mentioned above. The environment of the fabricated region of interest is mapped by taking lower magnification images (down to 312 times). See Table 1 for an overview of the available magnifications. The region of interest is kept in the centre of the images in order to know its position in low-magnification graphs that do not resolve the nanostructure. Intrinsic sample features that appear in these images, like grain boundaries in opals, are used to act as markers for subsequent alignment purposes.

After the fabrication process, we want to examine the geometrical shape and arrangement of the realized material cavities in detail. As the carbon layer may blur the fine details, it is first removed using oxygen plasma, from a Tepla 300E, with typical parameters: 15 min duration, 300 W plasma power, 1.25 mbar pressure and 50% O_2 flow. For high-contrast imaging of this low-conductance sample, it is placed in a high-resolution SEM (LEO 1550, LEO Elektronenmikroskopie GmbH, Oberkochen, Germany[1]), operating at a low acceleration voltage (1–1.5 kV), a working distance of 3 mm and using the in-lens detector to collect secondary electrons for imaging. See Table 1 for the available magnifications.

Recovery of our region of interest requires the following steps. First, the edges of the sample's substrate are carefully aligned parallel to the (x,y) translation axis of the sample positioner. Subsequently, the (x,y) coordinates, relative to the substrate corners, that were obtained during the FIB session are utilized to approach the region of interest to within about 50 μm. Using the SEM at a relatively low magnification (down to 84 times), we visually compare the SEM picture and the

[1] Currently: Carl Zeiss NTS, Oberkochen, Germany

images that were taken with the FIB. When intrinsic structural features on the surface of the sample are recognized in both the FIB and SEM images, it is possible to align to the exact location of the region of interest. Again, spatial (x,y) coordinates of the material nanocavities relative to two corners of the substrate are recorded. Subsequently, images at various magnifications are taken with the SEM in addition to the images from the FIB process. After recovery of the nanostructure, it was studied in detail using larger magnifications (up to 266 000 times).

After the geometry has been examined, we want to study optical properties of the material cavities. Two different optical microscopes are used, see Table 1 for an overview of the possible magnifications. Bright-field optical microscope imaging is performed with a Nikon Eclipse ME600L microscope and CFI LU Plan BD objectives (Uvikon, Bunnik, The Netherlands). A DXM-1200F digital camera is equipped to this microscope for imaging purposes. To localize our region of interest, we use the relative coordinates and images from the SEM session in combination with a low magnification ($10\times$) objective. After a characteristic structural feature from the SEM images is recognized, we move the sample such that the region of interest is in the centre of the image and study the sample optically with larger magnification objectives (up to 100 times).

Reflectivity measurements with a high spatial resolution are performed using a home-built, sample-scanning confocal microscope. An infinity corrected microscope objective (Olympus, $40\times/0.60$NA $\infty/0$-2/FN22, Olympus Netherland BV, Zoeterwoude, The Netherlands) is used to focus white light on the sample and collect the reflected light. The reflected light is focused through a pinhole with a diameter of 25 μm and subsequently directed to a spectrometer. In the spectrometer, the light is dispersed by a glass prism and projected onto a liquid nitrogen cooled CCD detector (Princeton Instruments, Spec-10:100B, Roper Scientific, Vianen, The Netherlands). In front of the pinhole, a flip mirror can be used to look at the sample with a CCD camera for alignment purposes. This results in an area of $40 \times 40\,\mu m^2$ that is imaged on a television screen. The sample is mounted on an (x,y) scanning piezostage (Physik Instrumente, P-740.20, ALT, Best, The Netherlands). A manual (x,y) stage is mounted on this piezostage to provide additional translation length. Using the relative (x,y) coordinates and images available from the FIB and SEM sessions, we are able to recognize characteristic features like grain boundaries on the sample. As the location of the region of interest is known with respect to these features, we track the sample on the television screen, while translating it such that the domain with the nanocavities comes into view.

After the alignment to the region of interest, the area reflectance of the sample's surface is collected by scanning the sample line by line through the focus of the objective, using the piezostage. The measured reflectance spectra are divided by the reflectance measured from a broad-band dielectric mirror (Thorlabs, BB1-E02) to obtain a reflectivity spectrum at every measured position. Additional software was written to select a wavelength range and represent the average reflectivity in this range as an area plot.

To calculate cross-correlations between two images, standard MATLAB (The MathWorks, Inc.) routines are used. Images with the same resolution are imported in MATLAB and converted to grayscale using the 'rgb2gray' function. Subsequently, the images are transformed to black and white images using 'im2bw', with a threshold value obtained by using 'graythresh' on the grayscale images. Finally, the black and white images are inverted and used as input for the normalized cross-correlation function 'normxcorr2'.

Results and discussion

The principal results of our deterministic method to study the same region of interest in various experimental setups are combined in Fig. 1. Figure 1(a) shows an image taken with the FIB workstation during fabrication. The individual silica spheres in the opal are recognized and near the centre one sees an array of seven milled spheres. Before the sample leaves the FIB workstation, low magnification pictures are taken in

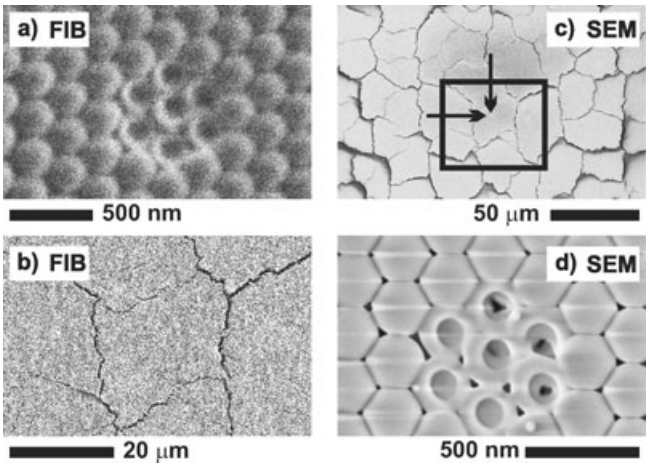

Fig. 1. (a) Micrograph obtained *in situ* during focused ion beam milling using a magnification of 65 000 times. Individual silica spheres ($R = 113$ nm) are clearly visible. Near the centre of the image, holes are milled in seven spheres. To map the environment from these milled spheres, the magnification of the focused ion beam workstation is reduced to 2000 times. (b) Contains the micrograph with the obtained map. After fabrication, the sample is placed in a SEM. (c) High-resolution scanning electron micrograph at a magnification of 2000 times. The area with the domain from (b) is recovered and highlighted by the black rectangle. The arrows point towards the milled defects. Stress induced grain boundaries in the sample show up as meandering lines which are useful for sample orientation and positioning in both (b) and (c). (d) High-resolution scanning electron micrograph of the same hole array as shown in (a), depicted with a high magnification (266 000 times). The horizontal streaks and the non-roundness of the spheres are charging effects of the SEM caused by the low conductance of the samples' surface. The images are resized and reoriented for clarity.

order to map the surroundings of the nanostructure under study, see Fig. 1(b). Stress-induced cracks that arise during the drying process of the opal (Jiang *et al.*, 1999; Hartsuiker & Vos, 2008) are recognized as the thick, black meandering grain boundaries, which delineate single-crystal domains with unique, characteristic shapes. The morphology of these grains cannot be predicted *a priori*, which differs from structures in semiconductor industry (Woldering *et al.*, 2008) that are known by design. The shape of a grain boundary itself may be very distinct with respect to its vicinity because of its width or because it is relatively straight and running alongside many domains. For our opals, these grain boundaries provide the guidance needed to recover the position and orientation of the milled spheres in other experimental setups.

After the fabrication process, the sample is mounted in the SEM to study the detailed structure. Figure 1(c) shows the low-magnification SEM image that was taken to map the vicinity of the location to which we want to align. The domain from Fig. 1(b) is recognized and subsequently translated to the centre of the SEM image. For clarity, this domain is outlined by a black box. The material cavities manifest themselves as a single bright region marked by the arrows. The location of the material nanocavities is now recovered and the SEM is subsequently used at higher magnifications. The resulting SEM image in Fig. 1(d) shows exactly the same nanocavities as Fig. 1(a). Clearly, this SEM provides much sharper images and superior contrast compared with the images from the FIB station, making the SEM data superior, with these low-conductance samples. For instance, the SEM image shows that several voids completely perforate the sphere in which they were milled, since one can see the next layer of spheres below. Similar results are obtained for the polystyrene opals (data not shown).

Once the sample's structure is elucidated by SEM, we wish to study the nanostructure with a second, different setup such as an optical microscope. Figure 2 contains the optical microscope results. The bright-field image in Fig. 2 shows that the grain boundaries in the opal structure are visible in these optical images. The black box outlines the same crystal area as in Fig. 1(c). For this particular experiment, we found the material cavities by searching for the characteristic small triangular domain at the bottom right, inside this black box. The green colour of the sample is caused by optical Bragg diffraction (Míguez *et al.*, 1997), in agreement with a measured photonic stop band centred at 514 nm.

The map in Fig. 2(b) shows a high-resolution spatial distribution of the optical reflectivity of the domain that contains the milled holes. This map was measured by confocal microscopy, where the sample was scanned with a stepsize of 0.30 μm. To construct the graph, the results for a range of wavelengths are collected from the measured spectra. We chose 658.2–659.6 nm, which is a representative range corresponding to optical photon energies below the photonic stop band, hence the reflectivity is low, about 4–8%. Again,

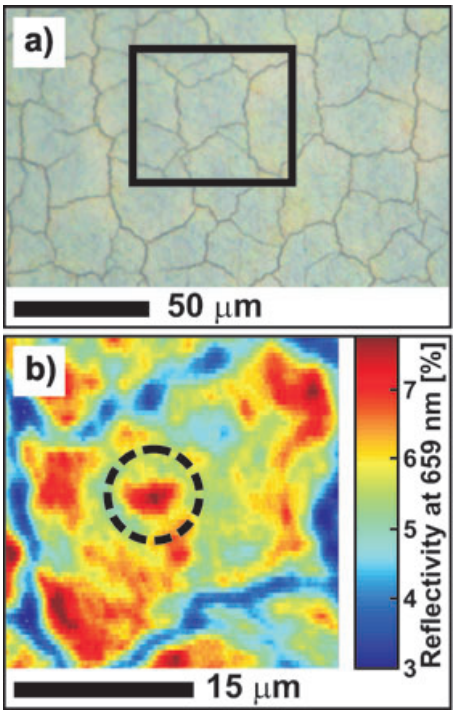

Fig. 2. (a) Bright-field optical microscope image of an opal of silica spheres ($R = 113$ nm). The crystal domain that contains our region of interest is recognized by cross-correlating this image with the area inside the rectangle from Figure 1(c). We outline the same area as a guide to the eye. The sample appears green due to the first-order photonic stop band from the opal. (b) Reflectivity map for wavelengths in the range of 658.2–659.6 nm, measured with the scanning confocal microscope in the crystal domain that contains the surface cavities. The location of the material nano-cavities is encircled by the dashed line and the size of the pixels is 0.30×0.60 μm^2. The reflectivity from the material cavities (about 8%, dark red) is higher than that of its vicinity.

the crystal domain is recognized by its boundaries, where the reflectivity is the lowest. Although the milled point defects are smaller than the spatial resolution of the experimental setup, the reflectivity from these nanostructures is distinct from its environment. For this wavelength, the reflectivity from the nanostructures appears to be higher than that of its vicinity. For photon energies above the photonic stop band, it appears that the reflectivity from the milled spheres is lower than that of the vicinity. Our results are in qualitative agreement with near-field scanning optical microscope experiments on opal surfaces with accidental point defects (Flück, 2003). A detailed analysis of the results is outside the scope of this paper.

For general usage, it would be convenient if our method could be extended by automating it. Therefore, images obtained with the different setups should be cross-correlated. Figure 3 shows the result of a normalized two-dimensional cross-correlation between the area outlined in Fig. 1(c) and the full Fig. 2(a). A clear dark spot appears where the images overlap best. The inset shows the side view of the area between

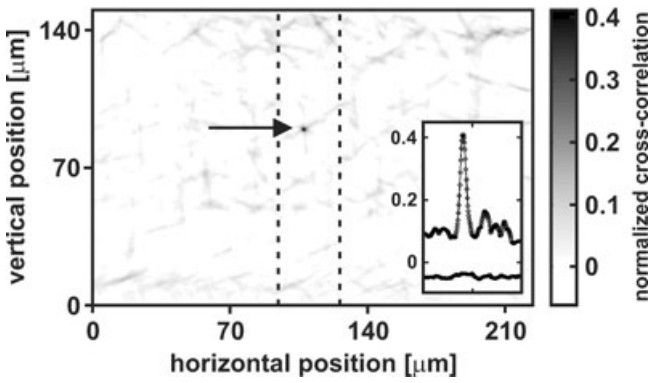

Fig. 3. Result of the normalized cross-correlation between the area inside the rectangle of the SEM image of Fig. 1(c) and the optical microscope image of Fig. 2(a). A clear dark spot appears at the position where the two images show the best overlap. This spot is indicated by the arrow. The inset is a zoom-in for horizontal positions between 95 and 126 μm (dashed lines). The upper data are the maxima and the lower data the minima on each horizontal position. The maximum of the correlation function is clearly peaked, and its value stands out of the maximum background by a factor of three.

the dashed lines and reveals that the location of best overlap clearly stands out of the maximum background by a factor of three. The full width at half maximum of this cross-correlation peak is 2.2 μm. After recovery of the region of interest with this precision, one can increase the magnification to improve the alignment.

Let us now briefly discuss limitations of the precision with which structures can be aligned in our setups. Similar limitations hold, in general, for all experimental setups. In the fabrication process with the FIB workstation, position uncertainties up to 50 μm are introduced while choosing the position of the substrate corners and because the substrate edges may not be completely parallel to the (x,y) translation axes of the stage. Similar uncertainties hold for the SEM setup. Therefore, these coordinates are not sufficient to recover the same nanostructure. In the wide-field microscope, it appeared to be difficult to manually align the substrate parallel to the axes of the translation stage. Furthermore, these stages exhibit hysteresis, and the accuracy of the rulers are two orders of magnitude less precise than the rulers used in the FIB and SEM. In case of the confocal microscope, it is inconvenient that the area that can be monitored during alignment is small. All together, these alignment issues pose practical demands on the low magnification FIB and SEM images that are used to recover the nanostructures. For these opals, we found maps that cover about 0.5×0.5 mm^2 to be very desirable.

Our method is straightforward and generally applicable in many research areas, especially in case of self-assembly and low-conductance samples. The method is very useful to align to different locations on a sample to reproduce experimental results. In biophysics, one may use the present approach to study individual bacteria, viruses, molecules or specific areas of cell walls and cells in general (Van Hulst *et al.*, 2000; Orrit, 2002). The attachment of wire bonds to nanostructures may also be established with the help of this method.

Conclusions

In this paper, we have shown how to recover deterministically fabricated single nanostructures in various setups for non-contact experiments. We are able to probe these structures in a variety of ways without the need of alignment markers, which may damage these structures. This enables the use of samples that are created solely by self-assembly. Structures smaller than the spatial resolution of the experimental setup can be probed, as was shown with the use of the optical microscopes. The orientation of the fabricated nanostructure in the setup is revealed as well. Spatial maps are essential to find the nanostructures. In addition to these maps (x,y) coordinates relative to the corners of the sample are used to facilitate the alignment process. Furthermore, cross-correlation techniques were introduced as a possible approach to automate the alignment procedure. The experimental method discussed in this paper was successfully used to align nanometre sized cavities on poorly conducting silica and polystyrene opal photonic crystals. In general, the performance of non-contact measurements on one or several experimental setups can benefit from our approach.

Acknowledgements

The authors thank Patrick Johnson and Sander Tans for useful discussions and anonymous referees for helpful comments. We are grateful to Vinod Subramaniam for his support. This research was supported by NanoNed, a nanotechnology programme of the Dutch Ministry of Economic Affairs, and by a VICI fellowship from the 'Nederlandse Organisatie voor Wetenschappelijk Onderzoek' (NWO) to W.L.V. This work is also part of the research programme of the 'Stichting voor Fundamenteel Onderzoek der Materie' (FOM), which is financially supported by the NWO.

References

Badolato, A., Hennessy, K., Atatüre, M., Dreiser, J., Hu, E., Petroff, P.M. & Imamoğlu, A. (2005) Deterministic coupling of single quantum dots to single nanocavity modes. *Science* **308**, 1158–1161.

Benkart, P., Heittmann, A., Huebner, H. & Ramacher, U. (2005) 3D chip stacking technology using through-chip interconnects. *IEEE Design Test Comput.* **22**, 512–518.

Flück, E. (2003) *Local interaction of light with periodic photonic structures*, PhD Thesis, University of Twente, ISBN: 90-365-1929-2.

Hartsuiker, A. & Vos, W.L. (2008) Structural properties of opals grown with vertical controlled drying. *Langmuir* **24**, 4670–4675.

Hla, S.-W. (2005) Scanning tunneling microscopy single atom/molecule manipulation and its application to nanoscience and technology. *J. Vacuum Sci. Tech. B* **23**, 1351–1360.

Jiang, P., Bertone, J.F., Hwang, K.S. & Colvin, V.L. (1999) Single-crystal colloidal multilayers of controlled thickness. *Chem. Mater.* **11**, 2132–2140.

Koppens, F.H.L., Buizert, C., Tielrooij, K.J., Vink, I.T., Nowack, K.C., Meunier, T., Kouwenhoven, L.P. & Vandersypen, L.M.K. (2006) Driven coherent oscillations of a single electron spin in a quantum dot. *Nature* **442**, 766–771.

López, C. (2006) Three-dimensional photonic bandgap materials: semiconductors for light. *J. Optics A* **8**, R1–R14.

Míguez, H., López, C., Meseguer, F., *et al.* (1997) Photonic crystal properties of packed submicrometric SiO_2 spheres, *Appl. Phys. Lett.* **71**, 1148–1150.

Novotny, L. & Hecht, B. (2006) *Principles of Nano-Optics*, Cambridge University Press, Cambridge.

Orrit, M. (2002) Single-molecule spectroscopy: the road ahead. *J. Chem. Phys.* **117**, 10938–10946.

Smith, D.R., Pendry, J.B. & Wiltshire, M.C.K. (2004) Metamaterials and negative refractive index. *Science* **305**, 788–792.

Tans, S.J., Devoret, M.H., Dai, H., Thess, A., Smalley, R.E., Geerligs, L.J. & Dekker, C. (1997) Individual single-wall carbon nanotubes as quantum wires. *Nature* **386**, 474–477.

Van Hulst, N.F., Veerman, J.A., Garcia-Parajo, M.F. & Kuipers, L. (2000) Analysis of individual (macro)molecules and proteins using near-field optics. *J. Chem. Phys.* **112**, 7799–7810.

Woldering, L.A., Otter, A.M., Husken, B.H. & Vos, W.L. (2006) Focused ion beam milling of nanocavities in single colloidal particles and self-assembled opals. *Nanotechnology* **17**, 5717–5721.

Woldering, L.A., Tjerkstra, R.W., Jansen, H.V., Setija, I.D. & Vos, W.L. (2008) Periodic arrays of deep nanopores made in silicon with reactive ion etching and deep UV lithography. *Nanotechnology* **19**, 145304: 1–11.

